Enhancement of polar anchoring strength in a graphene-nematic suspension and its effect on nematic electro-optic switching

Rajratan Basu

Phys. Rev. E **96**, 012707 — Published 27 July 2017

DOI: 10.1103/PhysRevE.96.012707

Polar anchoring strength enhancement in a graphene-nematic suspension and its effect on the nematic electro-optic switching

Rajratan Basu*

Department of Physics, Soft Matter and Nanomaterials Laboratory,

The United States Naval Academy, *Annapolis*, *MD 21402*, *USA*.

A small quantity of monolayer graphene flakes is doped in a nematic liquid crystal (LC), and the effective polar anchoring strength coefficient between the LC and the alignment substrate is found to increase by an order of magnitude. The hexagonal pattern of graphene can interact with the LC's benzene rings via π–π electron stacking, enabling the LC to anchor to the graphene surface homogeneously (i.e. planar anchoring). When the LC cell is filled with the graphene-doped LC, some graphene flakes are preferentially attached to the alignment layer and modify the substrate's anchoring property. These spontaneously deposited graphene flakes promote planar anchoring at the substrate and the polar anchoring energy at alignment layer is enhanced significantly. The enhanced anchoring energy is found to impact favorably on the electro-optic response of the LC. Additional studies reveal that the nematic electro-optic switching is significantly faster in the LC + graphene hybrid than that of the pure LC.

*Electronic address: basu@usna.edu

I. Introduction

The interaction of nematic liquid crystals (LC) with the alignment substrates in an LC cell is a very interesting problem pertinent to their electro-optic characteristics—which are technologically important for their applications in electro-optical display technology [1,2]. The alignment substrate in the cell orients the LC director along a particular orientation. An external electric field then can deviate the director from its initial orientation. The energy cost of this deviation from a planar orientation to a homeotropic orientation is characterized by the polar anchoring strength coefficient, W_θ. The polar anchoring strength is an important parameter for an LC cell because it influences the LC's electro-optic properties, such as the orientational threshold voltage and response time [3]. In this paper, we experimentally show that the presence of a small quantity of monolayer graphene flakes in a nematic LC significantly enhances the effective W_θ of the hybrid, and results in an accelerated electro-optic switching response.

Graphene is a crystalline allotrope of carbon with 2-dimensional properties. The carbon atoms in a graphene sheet are densely packed in a regular sp^2-bonded atomic-scale hexagonal pattern. This 2-dimensional hexagonal nanostructure of graphene makes it an interesting and important nanomaterial to study various LC—nanomaterial interactions along a new direction. For example, the presence of graphene can reduce the LC's pretilt angle at the substrate [4]. Transparent graphene-conducting-layers can be used as electrodes [5] to produce high transmittance liquid crystal displays [6,7]. Graphene flakes can reduce the LC's rotational viscosity by trapping free ions in the LC [8]. The honeycomb graphene surface can be used to enhance the spontaneous polarization in a ferroelectric liquid crystal [9]. Graphene flakes can enhance the orientational order [10] and dielectric anisotropy [11] in a nematic phase. The strain chirality of graphene surface can propagate into the LC, exhibiting an electroclinic effect in the

smectic-*A* phase and a macroscopic helical twist of the LC director in the nematic phase [12,13]. Dielectric spectroscopy of graphene-oxide doped LC reveals a noncollective relaxation which is absent in the pure LC [14]. Finally, graphene-oxide can improve the physiochemical properties of nematic LCs [15]. Therefore, studying the multifaceted interactions between LC and graphene has been an intriguing and active topic of research in recent years.

II. Experiments, Results, and Discussions

The pristine graphene (GP) sample in ethanol solvent was obtained from Graphene Supermarket, Inc. The graphene sample contained more than 97% of monolayer flakes (with a small fraction of multilayer flakes) of an average thickness of 0.35 nm and an average lateral size of 550 nm. The ethanol + GP solution was first remixed by a micro-homogenizer tip of 5 mm diameter at 35000 rpm for 5 min, followed by sonication for 4 h. The liquid crystal E7 (obtained from EMD Millipore Corporation, T_{NI} = 60.5^{o} C) then was added to the ethanol + GP and sonicated for 5 h, allowing the LC to dissolve completely into the solution. The ethanol was evaporated slowly at an elevated temperature. Finally, the LC+GP was degassed under a vacuum for 1 h, leaving a pure LC+GP mixture of 2.5×10^{-3} wt%. For consistency, the pure LC was also treated the same way, such as dissolving in ethanol followed by a slow evaporation and degassing. Commercially manufactured planar and homeotropic LC cells (from *Instec, Inc*.) with a 1 cm^2 semitransparent indium tin oxide (ITO) coated area and a d = 15 μm spacing were used for the polar anchoring strength measurements. The electro-optic switching response of the LC was performed using planar LC cells (*Instec, Inc*.) with a 0.25 cm^2 semitransparent ITO coated area and a d = 5 μm spacing. The graphene-doped LC cell was examined using a polarizing optical microscope. The optical micrographs revealed uniform nematic textures, like

that of the pure LC cell, indicating a uniform director field. Thus, at least on the length scales resolvable by visible light, the structure of graphene-aggregates must be small enough that they do not significantly perturb the director field due to their low concentration and uniform dispersion.

The nematic phase shows dielectric anisotropy, $\Delta\varepsilon = \varepsilon_{\parallel} - \varepsilon_{\perp}$, where $\varepsilon_{\parallel}$ and $\varepsilon_{\perp}$ are the dielectric components parallel and perpendicular to the nematic director, respectively. In a uniform planar cell configuration, the nematic director of a positive anisotropic ($+\Delta\varepsilon$) LC, like E7, is initially aligned perpendicular to the applied electric field $\vec{E}$, but the director can reorient parallel to $\vec{E}$ if the field magnitude is above some critical threshold—which is the essence of the Fréedericksz transition. The reorientation process of the nematic director, above the threshold field, occurs because the director experiences a torque $\propto \Delta\varepsilon\, E^2$ in the presence of $\vec{E}$. The capacitive measurement as a function of the applied voltage across the cell can reveal this LC reorientation process.

The polar anchoring strength coefficient, W_θ (for a small pretilt angle, $\theta_p < 5^o$) can be defined as [16]

$$W_\theta = \frac{2\,V_{th}^2}{A\,\pi^2}\frac{(C_{HT}-C_{PL})^2}{C_{PL}}\frac{1}{\left[1-\left(\frac{C_{PL}}{C_{HT}}\right)_{V\to\infty}\right]} \qquad (1)$$

where V_{th} is the Fréedericksz threshold voltage of the LC in the planar cell, A is the active area of the cells, C_{HT} is the capacitance of the LC filled homeotropic cell, C_{PL} is the capacitance of the LC filled planar cell for $V < V_{th}$. For this measurement, both the cells must have the same active area, A and thickness, d. In the denominator, $\left(\frac{C_{PL}}{C_{HT}}\right)_{V\to\infty}$ is the capacitance ratio of the planar cell to the homeotropic cell for a very high voltage limit. Note that for a positive anisotropic ($+\Delta\varepsilon$)

LC, C_{HT} does not change at the high voltage limit as the LC does not undergo Fréedericksz transition in the homeotropic cell. For the planar cell, C_{PL} at the high voltage limit can be determined from the C vs V^{-1} curve. For more accurate measurement of W_θ, Eq. 1 can be rewritten using the dielectric components of the LC, $\varepsilon_\parallel = \frac{d\, C_{\mathrm{HT}}}{A\, \varepsilon_o}$ and $\varepsilon_\perp = \frac{d\, C_{\mathrm{PL}}}{A\, \varepsilon_o}$, as

$$W_\theta = \frac{2\,\varepsilon_0 V_{th}^2}{d\,\pi^2}\frac{(\varepsilon_\parallel - \varepsilon_\perp)^2}{\varepsilon_\perp}\frac{1}{\left[1-\frac{\varepsilon_\parallel^{extp}}{\varepsilon_\parallel}\right]} \qquad (2)$$

where ε_0 the is free space permittivity, $\left(\frac{C_{\mathrm{PL}}}{C_{\mathrm{HT}}}\right)_{V\to\infty} = \frac{\varepsilon_\parallel^{extp}}{\varepsilon_\parallel}$, and $\varepsilon_\parallel^{extp}$ can be determined from the *extrapolated* intercept of the ε vs V^{-1} curve for the planar LC cell, as shown in Figure 1. An Automatic Liquid Crystal Tester (*Instec*, *Inc.*) was used to measure the capacitance of the empty cells and filled cells at 1000 Hz. Then the dielectric components were obtained using the ratio of the filled cell capacitance to the empty cell capacitance: $\varepsilon_\parallel = \frac{C_{\mathrm{HT}}}{C_{\mathrm{HT\_empty}}}$ and $\varepsilon_\perp = \frac{C_{\mathrm{PL}}}{C_{\mathrm{PL\_empty}}}$ (for $V < V_{\mathrm{th}}$). Equation 2 eliminates the error due to any small mismatch in d and A between the planar and homeotropic cells by introducing their empty cell capacitances. Figure 1(a) shows the dielectric constant ε for E7 and E7+GP samples as a function of rms voltage, obtained from the planar cells. Both the samples exhibit a typical Fréedericksz transition. The inset in Fig. 1(a) shows V_{th} for both the samples. Figure 1(b) shows ε vs V^{-1} for E7 and E7+GP samples. The solid lines represent the linear fit in the linear regime. The extrapolated Y-intercept of the linear fit gives the value of $\varepsilon_\parallel^{extp}$, as shown in Fig.1(b).

After calculating the dielectric components from the appropriate LC cells, Eq. 2 was used to obtain W_θ. Figure 2 shows W_θ as a function of temperature for E7 and E7+GP samples, listed in the legend. At 30 °C, $W_\theta^{\mathrm{E7}} = 3.8 \times 10^{-5}$ J m^{-2} and $W_\theta^{\mathrm{E7+GP}} = 4.1 \times 10^{-4}$ J m^{-2}. Note that Figure

2 shows W_θ on a linear scale and the inset shows the same on a logarithmic scale. These two scales clearly depict the dramatic increase in W_θ and its pretransitional behavior when graphene flakes are doped in the LC. Note that the inset in Fig. 1(a) shows that V_{th} for the E7+GP is higher than that of E7, indicating an increase in effective W_θ for the hybrid sample. No temperature hysteresis in W_θ for the E7+GP sample was observed.

To shed light on this significant increase in effective W_θ for the E7+GP hybrid, we first need to understand the anchoring mechanism of the LC molecules on the graphene surface. It has been shown that LC molecules can anchor to the *honeycomb* pattern of graphene [17,18] or carbon nanotubes [19,20,21,22,23,24,25,26], employing the π–π electron stacking. Density-functional calculations suggest that this anchoring is further strengthened with a binding energy of -2.0 eV by electrostatic energy due to a considerable amount of charge transfer from the LC molecule to the honeycomb pattern [20,21]. Figure 3(a) and (b) illustrate the π–π stacking interaction that arises due to the overlap of the LC's benzene rings on the graphene-honeycomb structure. However, it is difficult to visualize the effect of this strong interaction in an LC+GP colloidal system. Therefore, we have studied the LC alignment mechanism on a CVD-grown monolayer graphene film on a copper foil. It is known that between two crossed polarizers, a *bright state* with the maximum transmitted intensity appears when the planar-aligned LC nematic director is at 45^o with the polarizer (or with the crossed-analyzer). A *dark state* is achieved if the director is parallel to the polarizer (or to the crossed-analyzer). Figure 3(a) schematically illustrates that the LC director on graphene is orientated at 45^o with respect to the crossed polarizer and analyzer – which results in a bright state. When the system is rotated through 45^o, the director orients parallel to the analyzer (see Fig. 3(b)) – which leads to a dark state.

The CVD-grown graphene film on a copper foil was obtained from Graphene Supermarket, Inc. The graphene film was continuous, with irregular holes and cracks. In addition, the graphene film was polycrystalline (i.e. the presence of grains with different crystallographic orientation). A small droplet of E7 in the isotropic phase was first placed on the graphene film. The droplet then was blown away gently by a dust blower — which left a thin LC layer on the graphene surface. The LC coated graphene on the copper substrate then was heated up in the isotropic phase to get rid of any residual order from the coating process and then slowly cooled down to the nematic phase. The alignment of the LC on graphene film then was studied by reflected crossed polarized microscopy by observing the bright to dark transitions as the sample was rotated over 135^{o}. After coating the thin LC layer on the graphene film, different crystallographic graphene domains with grain boundaries became clearly visible. Figure 3(c), (d), (e), and (f) show the microphotographs at three different relative angles, 0^{o}, 45^{o}, and 90^{o}, with respect to the crossed polarizers. The highlighted domain intensity was tracked as the sample was rotated over 135^{o} under the reflected crossed polarized microscope. Figure 3(d) shows that after rotating 45^{o}, the highlighted domain becomes dark. Figure 3(e) depicts that after rotating 45^{o} more (i.e. a total of 90^{o} from the initial state), the highlighted domain becomes bright again. Figure 3(f) shows the normalized intensity of the highlighted domain as a function of the angle of rotation. These results suggest that the LC, on graphene, can achieve a planar aligned state, which can transit from dark to bright when rotated by 45^{o}. This planar aligned state is employed by the strong π–π electron stacking. This interaction still exists in the LC+GP colloidal system.

During the filling process of the LC cell, possibly some monolayer graphene flakes sediment down and/or get stuck to the substrates from the LC+GP mixture, and align themselves

horizontally on the substrates. When some graphene flakes are preferentially attached to the substrate, they promote planar anchoring, enhancing the overall polar anchoring of the system. A simple approach has been used to check the presence of graphene flakes, spontaneously deposited from the LC+GP hybrid, lying face on the substrates of the cell. The planar cells used for E7 and E7+GP were first disassembled and carefully washed using acetone to get rid of any LC. The bare alignment substrates of the cells were studied using transmitted microscopy and the microphotographs are shown in Figure 4. The bare alignment substrate used in the E7 cell is shown in Fig. 4(a). Only randomly dispersed spacer particles with uniform size are visible under the microscope. Figure 4(b) presents the bare alignment substrate used in the E7+GP cell. A careful observation reveals that in addition to the spacer particles, there present many dark spots much smaller than the spacer particles. These are small aggregated graphene flakes attached to the substrate. Figure 4(b) shows a spacer particle inside a dotted circle and graphene flakes inside a solid circle. Figure 4(c) presents a 7x magnified image of the dotted square region shown in Fig. 4(b). The presence of graphene flakes in small aggregates is clearly visible in Fig. 4(c). Presumably, there are many more graphene flakes present on the surface, but they are not visible under the microscope as they are attached to the substrate in non-aggregate forms. These results clearly indicate the presence of the adsorbed graphene layers on the alignment substrates used in the E7+GP cell. Figure 4(d) schematically shows a natural LC alignment on the alignment substrate. Figure 4(e) illustrates that the graphene-modified substrate enhances the average anchoring mechanism of the LC to the substrate due to the additional strong π–π electron stacking between graphene and LC. This mechanism leads to a strong increase in effective W_θ, as shown in Fig. 2.

Equation 2 shows that $W_\theta \propto (\Delta\varepsilon)^2$, where $\Delta\varepsilon (= \varepsilon_\parallel - \varepsilon_\perp)$ is the dielectric anisotropy. Therefore, a small increase in $\Delta\varepsilon$ can play a role in enhancing W_θ as well. From the capacitive measurements, $\Delta\varepsilon^2_{E7}$= 137 and $\Delta\varepsilon^2_{E7+GP}$= 155. Thus, we believe that $\Delta\varepsilon$ also plays a small part in increasing W_θ.

The graphene flakes that are suspended in the LC also contribute to the increase in W_θ. The capacitive data for the planar cells were used to extract the splay elastic constant, K_{11} using the Fréedericksz transition method [27] by fitting the capacitance (C) vs. voltage (V) graphs according to the equation, $\frac{C}{C_o} = \frac{2}{\pi}\sqrt{1+\gamma\sin^2\varphi_m}\frac{V_{th}}{V}\int_{\varphi_0}^{\varphi_m}\sqrt{\frac{(1+\gamma\sin^2\varphi)(1+\kappa\sin^2\varphi)}{\sin^2\varphi_m - \sin^2\varphi}}d\varphi$, where C_o is the zero-field capacitance, φ is the angle between the director and the substrate at V, φ_m is the maximum angle in the middle of the cell, φ_o is the pre-tilt angle, $\gamma = \Delta\varepsilon/\varepsilon_\perp$, $\kappa = (K_{33}/K_{11}) - 1$, K_{33} is the bend elastic constant, and V_{th} is the threshold voltage. Figure 5(a) shows K_{11} as a function of temperature for E7 and E7+GP samples. Away from the transition temperature, the E7+GP sample shows an increase in K_{11}. The suspended graphene flakes act as *local anchoring fields* in the LC due to the π–π stacking between graphene and LC. This mechanism increases the effective K_{11} in the graphene-nematic suspension. As $W_\theta \propto K_{11}$ [16], an increase K_{11} results in an increase in W_θ.

Note that the threshold voltage is characterized by $V_{th} = \pi\sqrt{(K_{11}/\varepsilon_o\Delta\varepsilon)}$. Since K_{11} and $\Delta\varepsilon$ both increase in the E7+GP sample, the effective change in V_{th} is small as shown in Fig. 1(a).

Now we will discuss the impact of this enhanced W_θ on the nematic switching response. The two characteristic times [28], rise (voltage on) and fall (voltage off), of the nematic director, considering W_θ, can be described as [29]:

$$\tau_{\text{rise}} = \frac{\gamma_1}{\Delta\varepsilon\, \varepsilon_o V^2 - K_{11}\pi^2}\left(d^2 + \frac{4\, d\, K_{11}}{W_\theta}\right),\ \tau_{\text{fall}} = \frac{\gamma_1}{K_{11}\pi^2}\left(d^2 + \frac{4\, d\, K_{11}}{W_\theta}\right) \qquad (3)$$

where γ_1 is the rotational viscosity, d is the cell thickness, $\Delta\varepsilon$ is the dielectric anisotropy, ε_0 the is free space permittivity, K_{11} is the splay elastic constant, and V ($>V_{\text{th}}$) is the driving applied voltage. τ_{rise} is the time the nematic director takes to rotate from planar to homeotropic configuration, when the voltage is turned on. Similarly, τ_{fall} is the time the director takes to relax back from homeotropic to planar configuration after the voltage is turned off.

The driving voltage, V is the dominating factor for τ_{rise}. When $V >> V_{\text{th}}$, the effect of W_θ on τ_{rise} is very small [29,30]. On the other hand, if the backflow in the cell is neglected, τ_{fall} is purely driven by the elastic interaction between the LC and the alignment substrate. In the weak anchoring limit ($W_\theta \sim 10^{-4}$ to 10^{-5} J m^{-2}), τ_{fall} is greatly influenced by W_θ as the term $\frac{K_{11}}{W_\theta}$ in τ_{fall} cannot be neglected [29,30]. Therefore, in the weak anchoring limit, an increase in W_θ results in a decrease in τ_{fall}.

Since the term $\frac{K_{11}}{W_\theta}$ influences τ_{fall}, we have studied this term for E7 and E7+GP samples as a function of temperature. The term $\frac{K_{11}}{W_\theta}$ was calculated using the results shown in Figure 2 and Figure 5(a), and then plotted as a function of temperature in Fig. 5(b). Clearly, $\frac{K_{11}}{W_\theta}$ is significantly reduced in the E7+GP sample, which is expected to accelerate τ_{fall}.

The field-induced nematic switching was studied from the electro-optic response of the LC cells. The optical setup consisted of a beam from a 5-mW He-Ne laser at wavelength 633 nm that passed through a polarizer, the cell, a crossed analyzer and into a nanosecond Newport photodetector. The beam was polarized at an angle of 45$^{\text{o}}$ with respect to the cell's rubbing

direction. The output of the detector was fed into a digital storage oscilloscope. A dc voltage pulse of 10 V (much higher than the threshold switching voltage) at a pulse interval of 20 Hz was applied across the cell and, the change in transmitted intensity as a function of time (both when the voltage was turned on and off) was detected by the oscilloscope. Transmitted responses for voltage on and voltage off were studied as a function of temperature for pure E7 and E7+GP samples. The setup was computer controlled and data acquisition was performed using LabVIEW® software.

Figure 6 represents the normalized transmitted intensity response (left *Y*-axis) as a function of time for voltage off and voltage on for E7 and E7+GP at $T = 30^{o}$C. The right *Y*-axis shows the applied voltage profile across the cells. The transmitted intensity increases as a function of time for E7 and E7+GP, as the applied voltage is turned off at time $t = 0$. It is apparent that E7+GP sample relaxes faster than pure E7 when the voltage is turned off. The time the transmitted intensity takes to rise from 10% to 90% of the maximum intensity, after the voltage is turned off, is defined as the optical switching off, τ_{off}. When the applied voltage is turned on at $t = 25$ ms, the transmitted intensity drops as a function of time for E7 and E7+GP. The time the transmitted intensity takes to drop from 90% to 10% of the maximum intensity, after the voltage is turned on, is defined as the optical switching on, τ_{on}. Note that τ_{rise} and τ_{fall} are not equal to the electro-optical responses τ_{on} and τ_{off}, respectively. However, the optical response is mainly due to the director's rotation after the voltage is turned on or off. Therefore, neglecting the backflow in the cell, one can write $\tau_{rise} \propto \tau_{on}$ and $\tau_{fall} \propto \tau_{off}$.

Figure 7(a) and (b) show τ_{on} and τ_{off}, respectively, as a function of temperature for E7 and E7+GP. Even though τ_{on} does not show any significant difference, τ_{off} shows a dramatic

decrease for the E7+GP sample. This accelerated switching response is mainly attributed to the significant enhancement in W_θ due to the presence of graphene in the LC and on the alignment substrate.

The presence of excess free ions can enhance the internal friction in the LC—which leads to an increase in γ_1 [31]. Several reports in the literature show that that the presence of carbon nanomaterials (such as carbon nanotubes, graphene flakes, fullerenes) in low-concentration in the LC can significantly reduce the free-ion concentration in the LC by the ion-trapping process—which results in a decrease in γ_1 of the LC media [4,7,8,31,32,33]. However, if the graphene-concentration increases significantly, the presence of the flakes themselves can enhance the internal friction, resulting in an increase in γ_1 [4]. In our experiment, the graphene concentration is very small ~ 10^{-3} wt%. We, therefore, believe that this low-concentration of GP can still trap free ions and reduce γ_1. Thus, in addition to the enhancement in W_θ, a decrease in γ_1 may also play a partial role in the faster response in the E7+GP sample.

III. Conclusion

It is presented that monolayer graphene flakes can change the anchoring property of the alignment substrate by self-deposition from the LC+GP mixture. The presence of monolayer graphene flakes on the alignment layer causes the polar anchoring strength to increase by an order of magnitude due to the strong the π–π electron stacking between the LC and graphene. The elastic force driven *fall* time of the nematic phase is accelerated significantly due to the strong anchoring between the LC, graphene, and the alignment substrate. Presented results are expected to advance the conceptions about, and methodology towards, nanoscale manipulation of LCs and LC-orientation control using their interactions with graphene.

Acknowledgements

This work was supported by the Office of Naval Research (Award No. N0001417WX01519) and the investment grant at the U.S. Naval Academy.

Figure Captions:

Figure 1: (a) Dielectric constant, ε for E7 and E7+GP as a function of V_{rms} at T = 30 ^{o}C. The inset shows the Fréedericksz threshold voltage, V_{th} for the samples. **(b)** Dielectric constant, ε for E7 and E7+GP as a function of $1/V_{\text{rms}}$ at T = 30 ^{o}C. The solid lines represent the linear fit in the high-voltage linear regime (as $1/V_{\text{rms}} \rightarrow 0$, $V_{\text{rms}} \rightarrow \infty$). The extrapolated Y-intercept of the linear fit gives the value of $\varepsilon_{\parallel}^{extp}$.

Figure 2: Polar anchoring strength coefficient, W_{θ} as a function of temperature for E7 and E7+GP on the linear scale. Typical error bars are shown. The dotted lines are guide-to-the-eye. The inset shows W_{θ} as a function of temperature for E7 and E7+GP on the logarithmic scale.

Figure 3: (a) A schematic representation of the alignment of nematic LC molecules on graphene due to π–π electron stacking. The ellipsoids are LCs and the black honeycomb structure is the graphene surface. The LC molecular structure is shown in the ellipsoid on the graphene surface. The π–π electron stacking is illustrated by matching the LC's benzene rings on the graphene-honeycomb structure. The nematic director ($\hat{n}$) is orientated at 45^{o} with respect to the crossed polarizer (P) and analyzer (A). This orientation, therefore, produces a bright state. **(b)** The system is rotated through 45^{o} and the nematic director ($\hat{n}$) is parallel to A — which produces a dark state. **(c)**, **(d)**, **(e)** Microphotographs of a thin layer of nematic LC on a monolayer graphene film on a copper substrate under a reflected crossed polarized microscope, showing a *bright*

state, a *dark state*, and a *bright state* of the *highlighted domain* at 0^o, 45^o, and 90^o, respectively, with respected to the crossed polarizers. **(f)** Normalized intensity of the highlighted domain as a function of the relative angle of rotation. The white bar in micrograph (e) presents 50 μm.

Figure 4: (a) Microphotograph of the bare alignment substrate used in the E7 cell. Randomly dispersed spacer particles with uniform size are visible. Two of them are highlighted with dotted circles. **(b)** Microphotograph of the bare alignment substrate used in the E7+GP cell. The dark spots, much smaller than the spacer particles, are graphene aggregates. These are small aggregated graphene flakes attached to the substrate. A spacer particle is highlighted inside a dotted circle and a few graphene flakes are highlighted inside a solid circle. **(c)** A 7x magnified image of the dotted square region of (b). A spacer particle is highlighted inside a dotted circle at the bottom left corner. All other smaller dark spots are graphene flakes in small aggregates.

Figure 5: (a) Splay elastic constant, K_{11} as a function of temperature for E7 and E7+GP. Typical error bars are shown. **(b)** $\frac{K_{11}}{W_\theta}$ as a function of temperature for E7 and E7+GP.

Figure 6: Electro-optic switching of E7 and E7+GP cells. The left *Y*-axis shows the normalized transmitted intensity as a function of time when an applied voltage is turned off at $t = 0$, and then turned on at $t = 25$ ms, for E7 and E7+GP, listed in the legend ($T = 30^o$ C). The right *Y*-axis shows the applied voltage profile across the cells.

Figure 7: (a) Optical switching on, τ_{on} and **(b)** optical switching off, τ_{off} as a function of temperature for E7 and E7+GP listed in the legend.

References:

[1] L.M. Blinov and V.G. Chigrinov, Electro-optic Effects in Liquid Crystal Materials (Springer-Verlag, New York, 1996)

[2] Sergey V. Pasechnik, Vladimir G. Chigrinov, and Dina V. Shmeliova, Liquid Crystals: Viscous and Elastic Properties (Wiley-VCH, Weinheim, Germany, 1999)

[3] X. Nie, R. Lu, H. Xianyu, T. Wu, S-T Wu, J. Appl. Phys. **95**, 5502 (2004).

[4] R. Basu, D. Kinnamon, N. Skaggs, and J. Womack, Journal of Applied Physics **119**, 185107 (2016).

[5] R. Basu and S. Shalov, Physical Review E **96**, 012702 (2017).

[6] P. Blake, P. D. Brimicombe, R. R. Nair, T. J. Booth, D. Jiang, F. Schedin, L. A. Ponomarenko, S. V. Morozov, H. F. Gleeson, E. W. Hill, A. K. Geim, and K. S. Novoselov, Nano Lett. **8**, 1704 (2008).

[7] Y. U. Junga, K. W. Parka, S. T. Hura, S. W. Choia, and S. J. Kanga. Liq. Cryst. **41**, 101 (2014).

[8] R. Basu, A. Garvey, and D. Kinnamon, Journal of Applied Physics **117**, 074301 (2015).

[9] R. Basu, Applied Physics Letters **105**, 112905 (2014).

[10] T. M. Alam and C. J. Pearce, Chemical Physics Letters **592**, 7 (2014).

[11] R. Basu, D. Kinnamon, and A. Garvey, Applied Physics Letters **106**, 201909 (2015).

[12] R. Basu, D. Kinnamon, and A. Garvey, Journal of Applied Physics **118**, 114302 (2015).

[13] R. Basu, D. Kinnamon, and A. Garvey, Liquid Crystals **43**, 2375 (2016).

[14] S. Al-Zangana, M. Iliut, M. Turner, A. Vijayaraghavan, I. Dierking, Advanced Optical Materials **4**, 1541 (2016).

[15] S. Javadian, N. Dalir, J. Kakemam, Liquid Crystals **42**, 1 (2017).

[16] A. Murauski, V. Chigrinov, A. Muravsky, F. S.-Y. Yeung, J. Ho, and H.-S. Kwok, Phys. Rev. E **71**, 061707 (2005).

[17] D. W. Kim, Y. H. Kim, H. S. Jeong, and H.-T. Jung, Nature Nanotechnology **7**, 29 (2012).

[18] M. A. Shehzad, D. H. Tien, M. W. Iqbal, J. Eom, J. H. Park, C. Hwang, and Y. Seo, Scientific Reports **5**, 13331 (2015).

[19] I.-S. Baik, S. Y. Jeon, S. H. Lee, K. A. Park, S. H. Jeong, K. H. An, and Y. H. Lee, Appl. Phys. Lett. **87**, 263110 (2005).

[20] K. A. Park, S. M. Lee, S. H. Lee, and Y. H. Lee, J. Phys. Chem. C **111**, 1620 (2007).

[21] S. Y. Jeon, K. A. Park, I. S. Baik, S. J. Jeong, S. H. Jeong, K. H. An, S. H. Lee, and Y. H. Lee, Nano **2**, 41 (2007).

[22] R. Basu and A. Garvey, Journal of Applied Physics **120**, 164309 (2016).

[23] R. Basu and G. S. Iannacchione, Applied Physics Letters **95**, 173113 (2009).

[24] R. Basu and G. S. Iannacchione, Physical Review E **81**, 051705 (2010).

[25] R. Basu, C.-L. Chen, and C. Rosenblatt, Journal of Applied Physics **109**, 083518 (2011).

[26] R. Basu, C. Rosenblatt, and R. Lemieux, Liquid Crystals **39**, 199 (2012).

[27] D. Demus, J. Goodby, G. W. Gary, H. –W. Spiess, V. Vill, Physical Properties of Liquid Crystals (Wiley-VCH, Weinheim, Germany, 1999).

[28] E. Jakeman and E. P. Raynes, Phys. Lett. **39A**, 69 (1972).

[29] X. Nie, R. Lu, H. Xianyu, T. X. Wu, and S. T. Wu, J. Appl. Phys. **101**, 103110 (2007).

[30] S. Y. Lu and L. C. Chien, Opt. Express **16**, 12777 (2008).

[31] H.Y. Chen, W. Lee, N.A. Clark, Appl. Phys. Lett. **90**, 033510 (2007).

[32] C.-W. Lee and W.-P. Shih, Mater. Lett. **64**, 466 (2010).

[33] R. Basu, Applied Physics Letters **103**, 241906 (2013).

Fig. 1

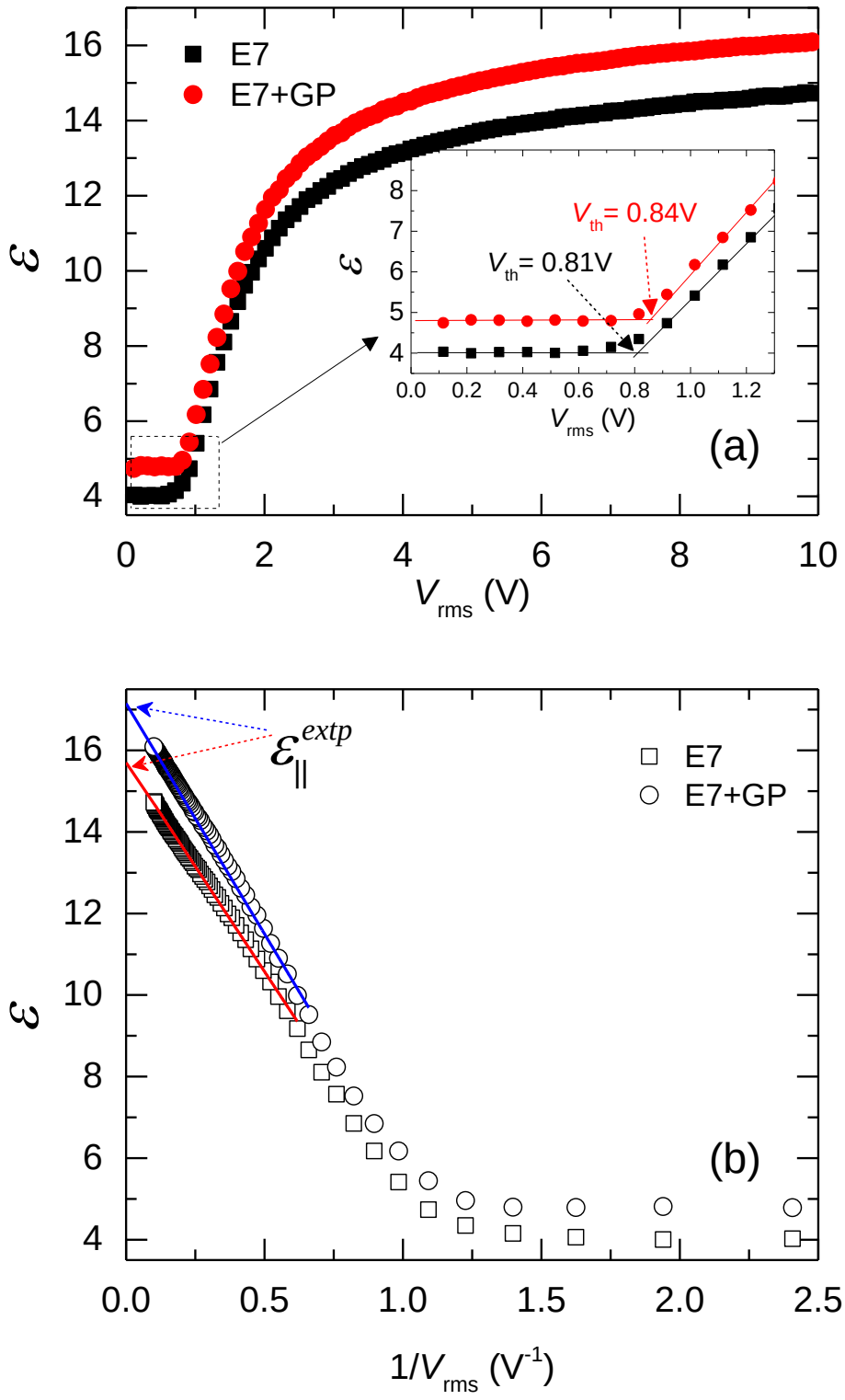
E7
E7+GP
ε
V_{rms} (V)
V_{th}= 0.84V
V_{th}= 0.81V
(a)
$\varepsilon_{\parallel}^{extp}$
1/V_{rms} (V^{-1})
(b)

Fig. 2

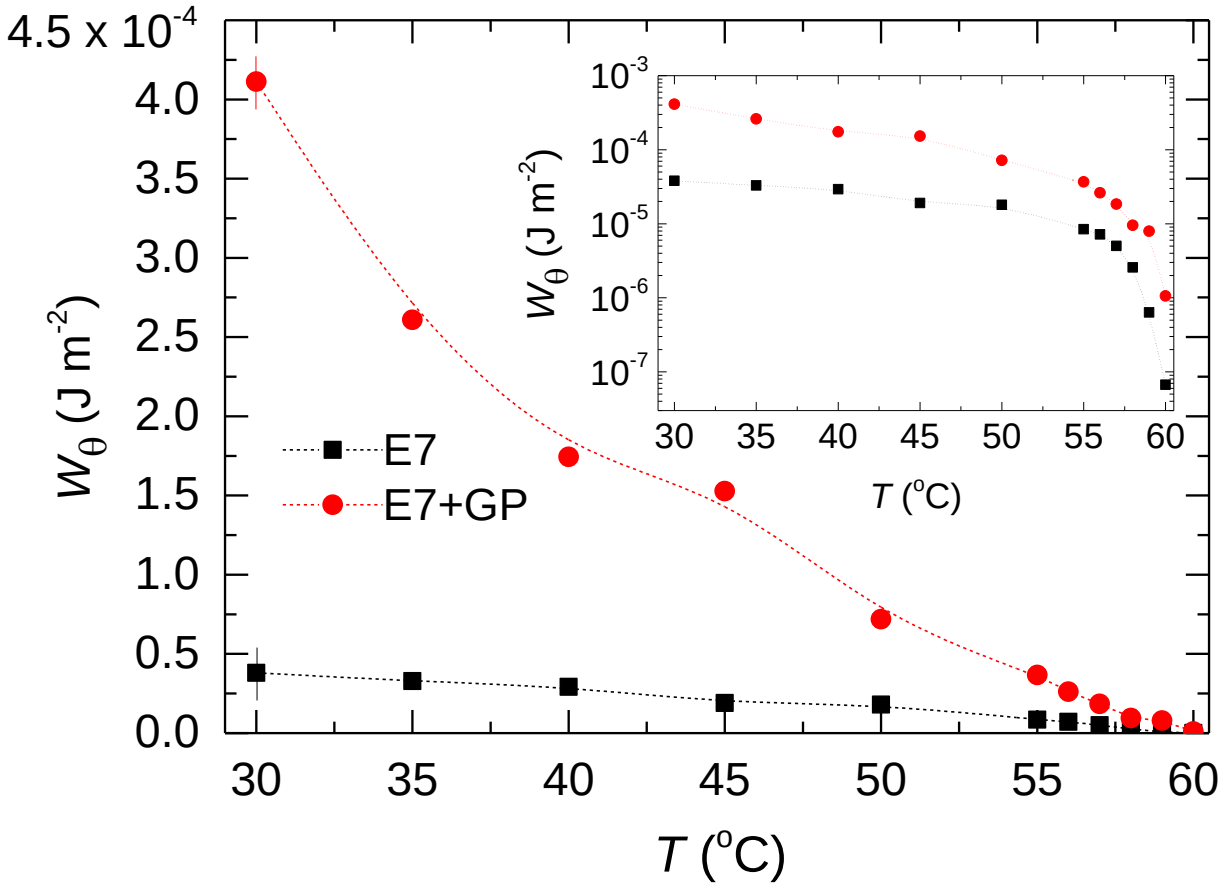
4.5 x 10-4
4.0
3.5
3.0
2.5
2.0
1.5
1.0
0.5
0.0
Wθ (J m-2)
E7
E7+GP
30
35
40
45
50
55
60
T (°C)
10-3
10-4
10-5
10-6
10-7
Wθ (J m-2)
30
35
40
45
50
55
60
T (°C)

Fig. 3

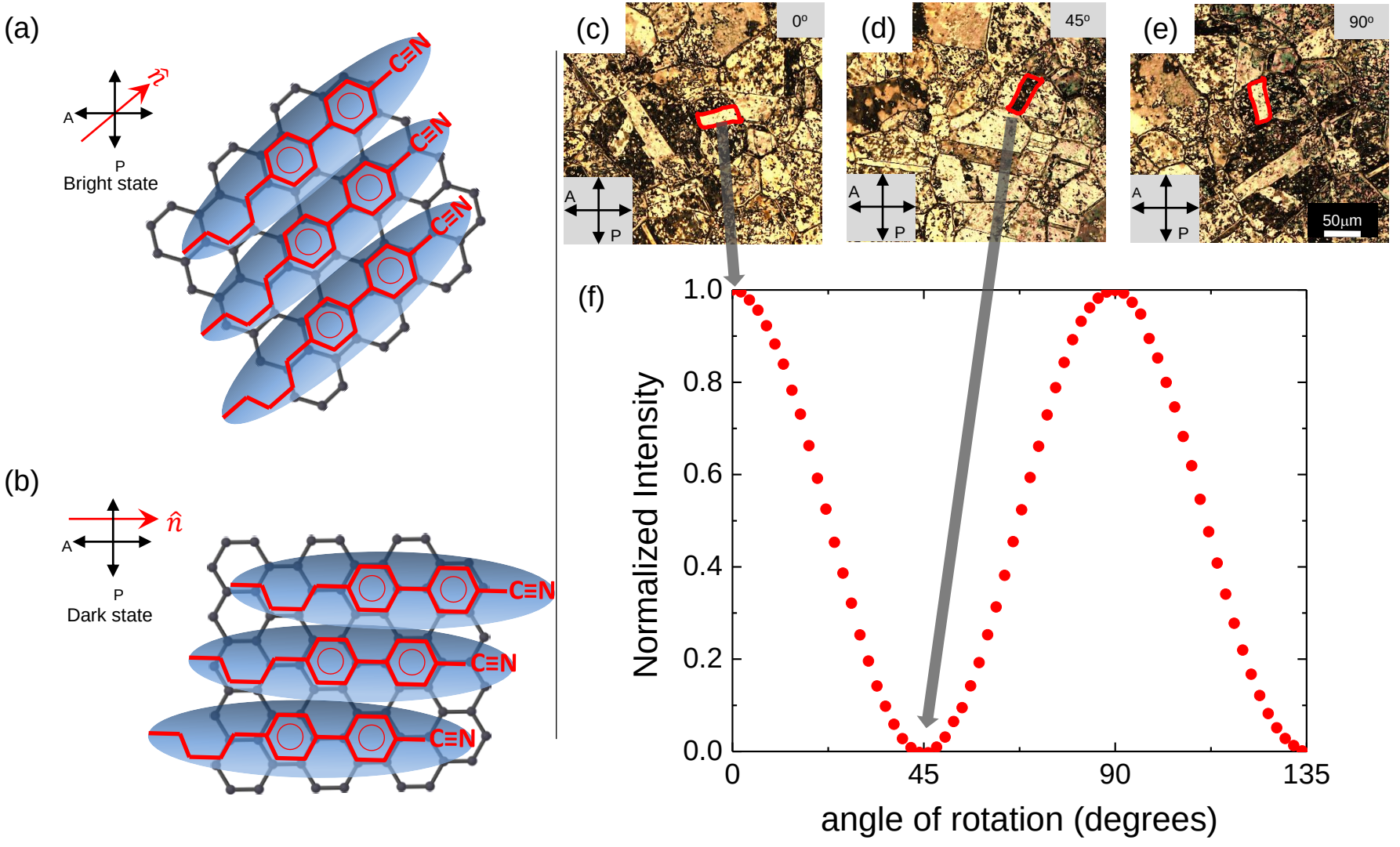
(a)
A
P
Bright state
C≡N
C≡N
C≡N
(b)
A
P
Dark state
C≡N
C≡N
C≡N
(c)
0º
A
P
(d)
45º
A
P
(e)
90º
A
P
50μm
(f)
Normalized Intensity
1.0
0.8
0.6
0.4
0.2
0.0
0
45
90
135
angle of rotation (degrees)

Fig. 4

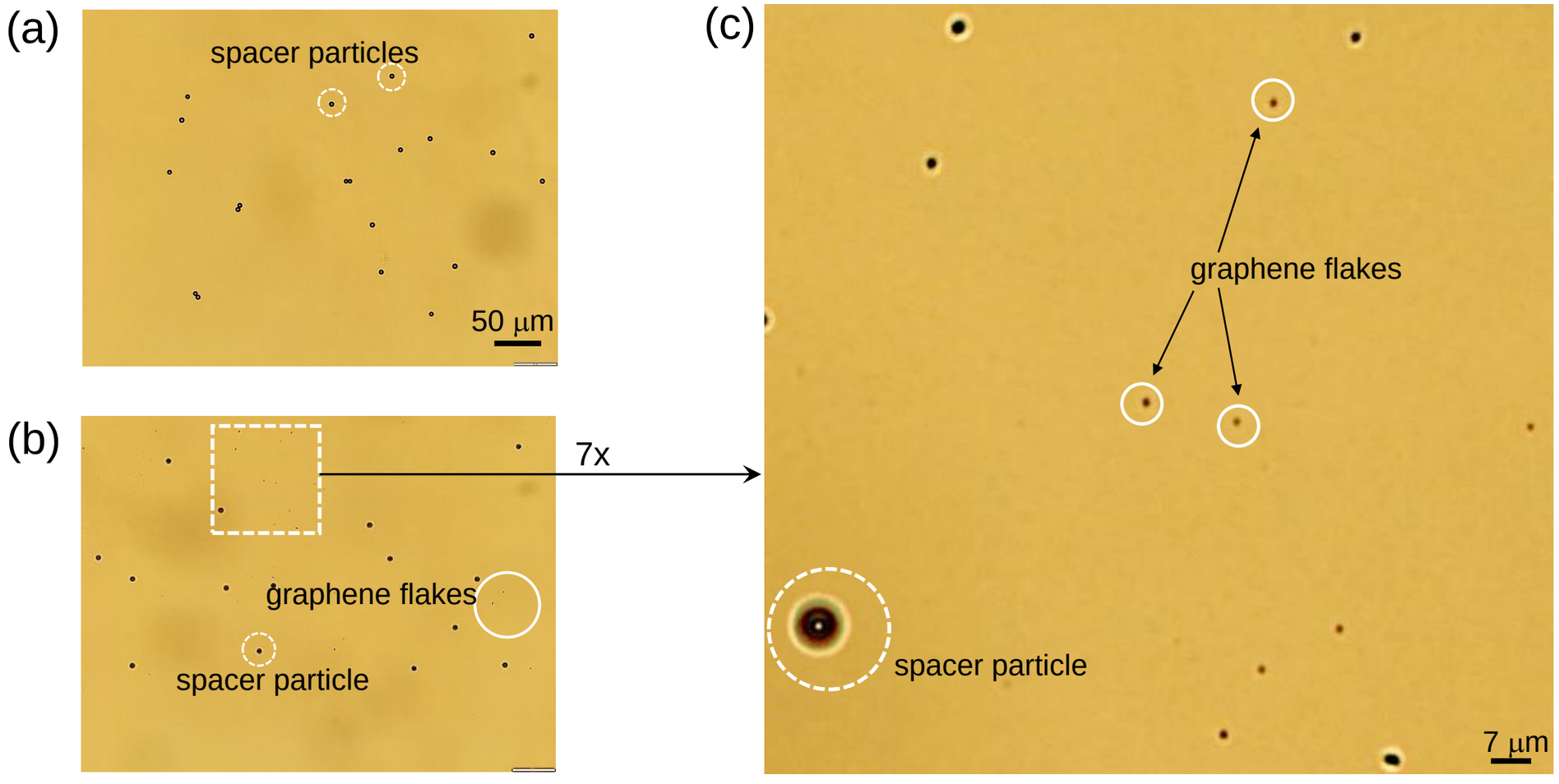
(a)
spacer particles
50 μm
(b)
7x
graphene flakes
spacer particle
(c)
graphene flakes
spacer particle
7 μm

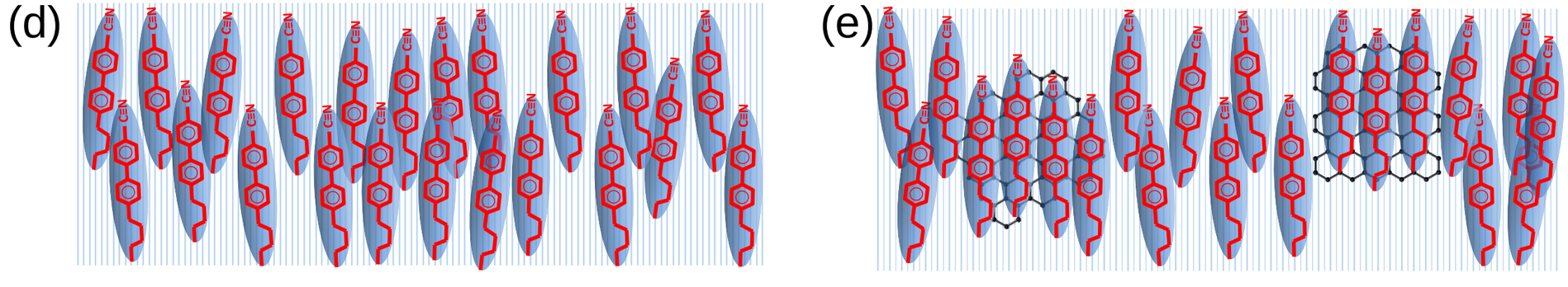
(d)
(e)

Fig. 5

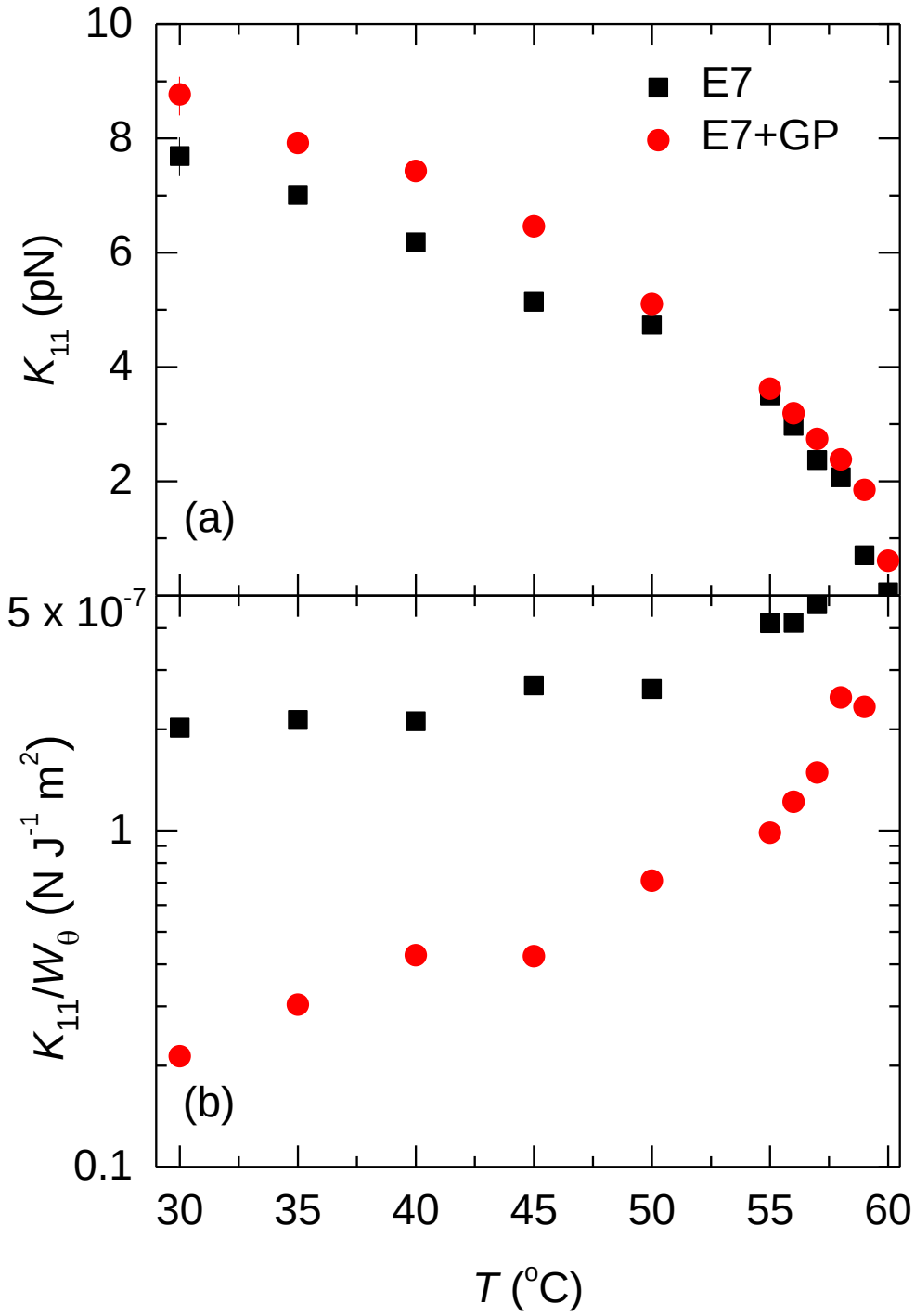
10
8
6
4
2
K_{11} (pN)
E7
E7+GP
(a)
5 x 10^{-7}
1
0.1
K_{11}/W_θ (N J^{-1} m^2)
(b)
30
35
40
45
50
55
60
T (^{o}C)

Fig. 6

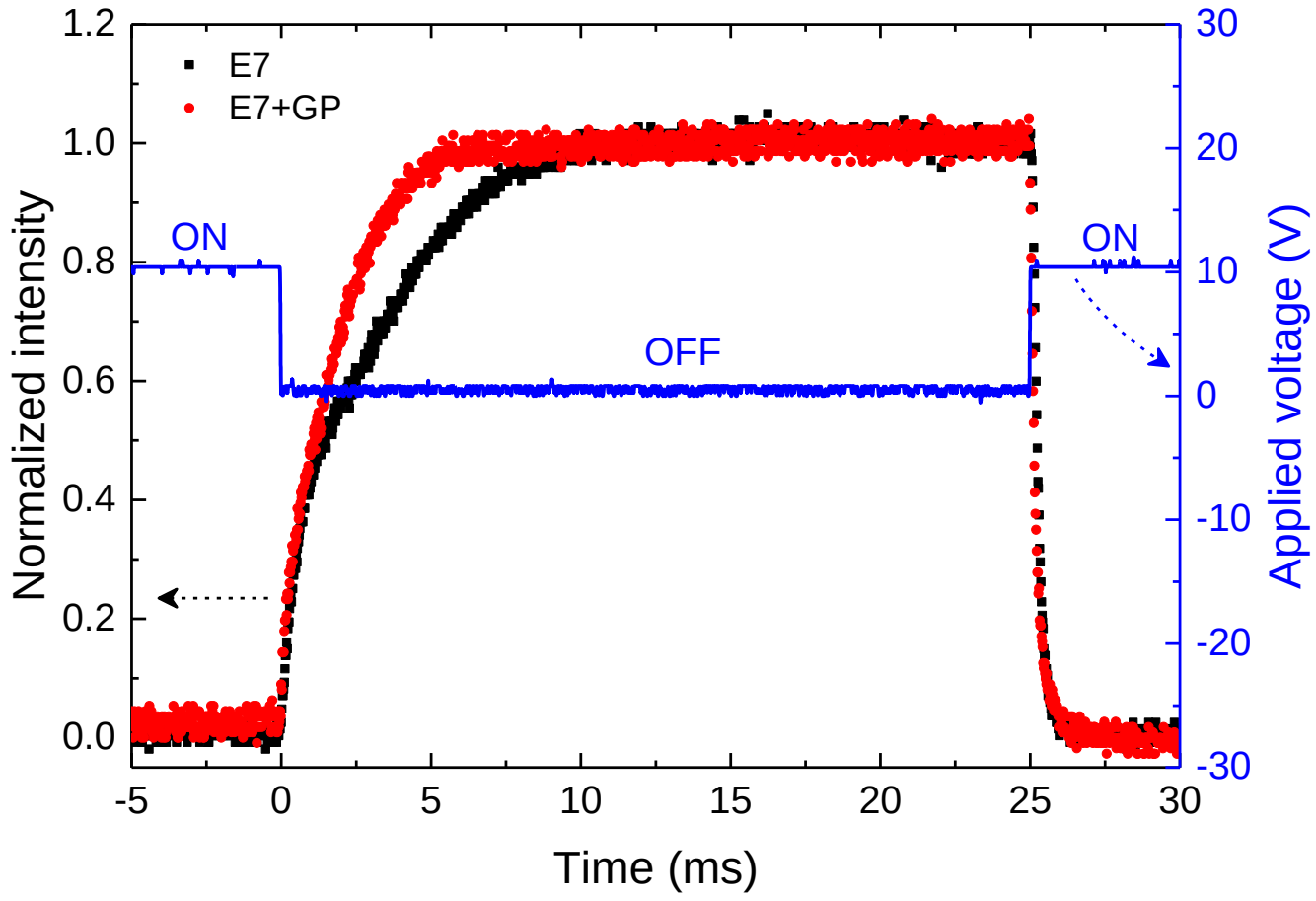
E7
E7+GP
ON
OFF
ON
Normalized intensity
Applied voltage (V)
Time (ms)
1.2
1.0
0.8
0.6
0.4
0.2
0.0
30
20
10
0
-10
-20
-30
-5
0
5
10
15
20
25
30

Fig. 7

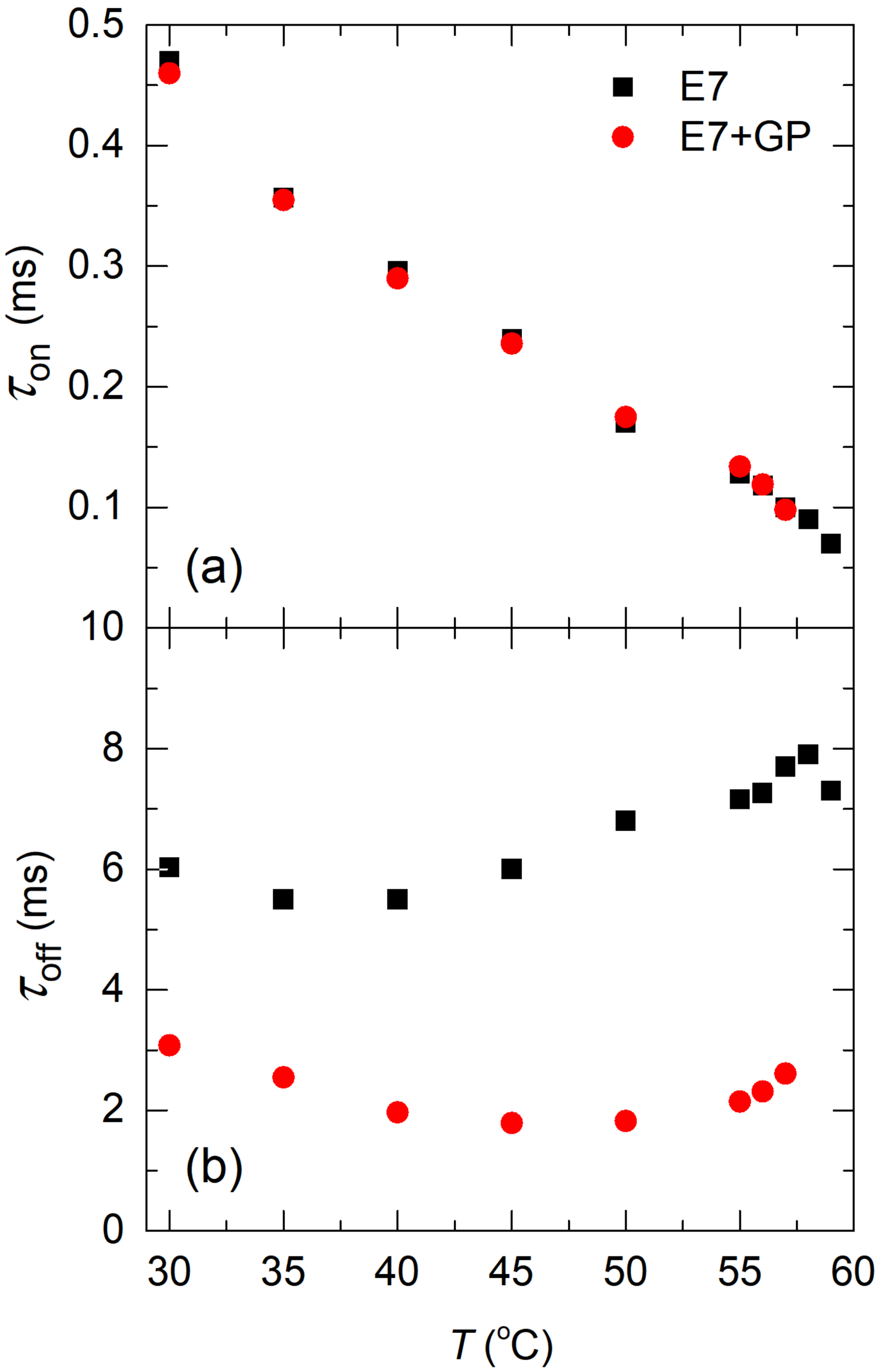
E7
E7+GP
τ_{on} (ms)
0.5
0.4
0.3
0.2
0.1
(a)
10
8
6
4
2
0
(b)
τ_{off} (ms)
30
35
40
45
50
55
60
T (°C)